

CORA: A Pathology Synthesis Driven Foundation Model for Coronary CT Angiography Analysis and MACE Risk Assessment

Jinkui Hao¹, Gorkem Durak¹, Halil Ertugrul Aktas¹, Ulas Bagci^{1,2}, Bradley D. Allen¹, Nilay S. Shah^{3,4}, and Bo Zhou^{1,*}

¹Department of Radiology, Northwestern University, Chicago, IL, USA

²Department of Biomedical Engineering, Northwestern University, Evanston, IL, USA

³Department of Cardiology, Northwestern University, Chicago, IL, USA

⁴Department of Preventive Medicine, Northwestern University, Chicago, IL, USA

**bo.zhou@northwestern.edu*

ABSTRACT

Coronary artery disease, the leading cause of cardiovascular mortality worldwide, can be assessed non-invasively by coronary computed tomography angiography (CCTA). Despite progress in automated CCTA analysis using deep learning, clinical translation is constrained by the scarcity of expert-annotated datasets. Furthermore, widely adopted label-free pretraining strategies, such as masked image modeling, are intrinsically biased toward global anatomical statistics, frequently failing to capture the spatially localized pathological features of coronary plaques. Here, we introduce CORA, a 3D vision foundation model for comprehensive cardiovascular risk assessment. CORA learns directly from volumetric CCTA via a pathology-centric, synthesis-driven self-supervised framework. By utilizing an anatomy-guided lesion synthesis engine, the model is explicitly trained to detect simulated vascular abnormalities, biasing representation learning toward clinically relevant disease features rather than dominant background anatomy. We trained CORA on a large-scale cohort of 12,801 unlabeled CCTA volumes and comprehensively evaluated the model across multi-center datasets from nine independent hospitals. Across diagnostic and anatomical tasks, including plaque characterization, stenosis detection, and coronary artery segmentation, CORA consistently outperformed the state-of-the-art 3D vision foundation models, achieving up to a 29% performance gain. Crucially, by coupling the imaging encoder with a large language model, we extended CORA into a multimodal framework that significantly improved 30-day major adverse cardiac event (MACE) risk stratification. Our results establish CORA as a scalable and extensible foundation for unified anatomical assessment and cardiovascular risk prediction.

Introduction

Coronary artery disease (CAD), driven by atherosclerotic plaque accumulation within the epicardial vasculature, remains the single leading cause of cardiovascular mortality globally, responsible for an estimated 17.9 million deaths annually¹. The clinical use of coronary computed tomography angiography (CCTA) for non-invasive evaluation of symptomatic patients is rapidly growing, and the utility of CCTA for primary atherosclerotic cardiovascular disease prevention is an important and active area of research²⁻⁴. The unique clinical value of CCTA lies in its ability to visualize not only luminal stenosis but also the underlying atherosclerotic plaque morphology, which is a critical and independent predictor of future myocardial infarction^{5,6}. Landmark randomized trials, including SCOT-HEART and PROMISE, have demonstrated that CCTA-guided management reduces major adverse cardiac events and improves long-term clinical outcomes^{7,8}. Despite this established efficacy, the clinical translation of CCTA remains constrained by an expanding interpretation burden: each examination demands 20–40 minutes of expert radiologist time⁹, and the global shortage of trained cardiac imaging readers is projected to worsen substantially over the next decade. The resulting bottleneck limits timely patient access to diagnostic imaging and exposes patients to clinically meaningful inter-observer variability, particularly for high-risk plaque features that are spatially subtle and easily overlooked during routine review¹⁰⁻¹².

A central obstacle to automated CCTA analysis lies in the extreme spatial sparsity of the pathological signal. Atherosclerotic plaques often occupy less than 1% of the total CCTA volume¹³, embedded within a complex background of myocardium, extra-cardiac fat, and contrast-enhanced blood pool. This imbalance fundamentally challenges standard

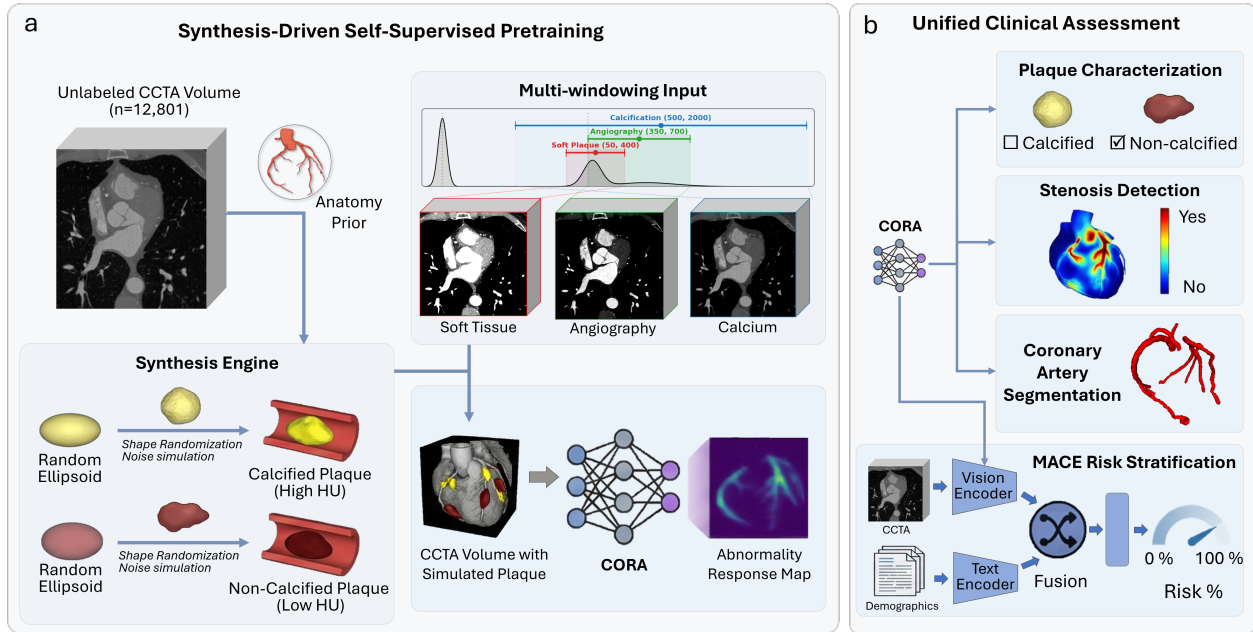


Figure 1. Overview of CORA and synthesis-driven pretraining framework. (a) Synthesis-driven self-supervised pretraining of CORA on large-scale unlabeled CCTA volumes. An anatomy-guided lesion synthesis engine generates diverse calcified and non-calcified plaque patterns with controlled morphology and attenuation, which are inserted into CCTA volumes to create simulated abnormality. Multi-windowing inputs capture complementary tissue characteristics across soft tissue, contrast-enhanced lumen, and calcium windows, enabling the encoder to learn pathology-centric representations and produce localized abnormality response maps. (b) Down-stream clinical assessment using the pretrained CORA encoder. A single foundation model supports multiple downstream tasks, including coronary plaque classification, stenosis detection, and coronary artery segmentation. For prognostic modeling, imaging representations are further integrated with patient demographic and clinical information through a multimodal fusion framework to enable major adverse cardiac event (MACE) risk stratification.

representation learning paradigms: models trained on such data are intrinsically biased toward the dominant anatomical structures that constitute the vast majority of image content, while systematically under-representing the subtle, spatially localized intensity variations that characterize clinically decisive vascular abnormalities. Consequently, current state-of-the-art approaches rely on multi-stage pipelines involving vessel detection, centerline extraction, and multi-planar reformatting¹⁴⁻¹⁸, which limits scalability and introduces error propagation across stages.

While deep learning has demonstrated promise in improving CCTA workflow efficiency¹⁹⁻²², the development of robust, end-to-end models for comprehensive CAD assessment remains a fundamental challenge. This challenge is compounded by the scarcity of expert-annotated datasets: accurate plaque characterization and stenosis grading require specialized expertise and remain subject to substantial inter-reader disagreement²³. The high cost of expert annotation has motivated substantial interest in self-supervised learning (SSL), which derives transferable representations from large collections of unlabeled data²⁴⁻²⁶. In 2D medical imaging domains, SSL-pretrained foundation models have demonstrated impressive downstream capabilities²⁷⁻³². However, the translation of these paradigms to 3D volumetric CCTA analysis has exposed a critical conceptual limitation. The dominant 3D SSL objective paradigms³³⁻³⁷, such as masked image modeling, emphasize global anatomical reconstruction. Emerging evidence suggests these approaches offer limited benefit for downstream clinical cardiovascular tasks, as they inherently sacrifice the representation of sparse, localized pathological signals in favor of background anatomy³⁸.

Here we develop CORA, a 3D vision foundation model for comprehensive cardiovascular risk assessment, designed to overcome these fundamental limitations through two conceptually distinct innovations. First, in place of generic anatomical reconstruction, CORA employs a synthesis-driven self-supervised paradigm: an anatomy-guided lesion synthesis engine generates realistic calcified and non-calcified plaque morphologies with controlled Hounsfield Unit

distributions and inserts them into unlabeled CCTA volumes, explicitly transforming pretraining into an abnormality detection task. This formulation directly biases encoder representations toward clinically relevant vascular pathology rather than dominant background anatomy. Second, CORA replaces standard single-channel normalization with a multi-windowing input strategy that simultaneously encodes tissue characteristics across soft tissue, contrast-enhanced lumen, and calcium windows, enabling discrimination between low-attenuation non-calcified plaques and high-density calcified lesions within a single forward pass—without requiring vessel segmentation or multi-planar reformatting as preprocessing.

We trained CORA on a large-scale cohort of 12,801 unlabeled CCTA volumes and systematically evaluated the model across multi-center datasets from nine hospitals. We benchmarked CORA on diagnostic tasks (coronary plaque characterization and stenosis detection) and anatomical tasks (coronary artery segmentation). We then extended CORA into a multimodal prognostic framework, coupling the imaging encoder with a large language model-based demographic encoder to predict 30-day major adverse cardiac events (MACE). We demonstrate that our CORA model outperforms carefully chosen state-of-the-art 3D foundation models across all benchmarking tasks. Ultimately, our results illustrate how pathology-centric pretraining establishes a highly generalizable foundation for unified anatomical assessment and long-term cardiovascular risk stratification from CCTA.

Results

Synthesis-driven pretraining biases CORA toward clinically relevant vascular pathology

To evaluate CORA across clinically diverse settings, we benchmarked it against baseline training from scratch and three state-of-the-art 3D vision foundation models, including MAE³⁹, VolumeFusion⁴⁰, and VoCo⁴¹, across four task categories: volume-level coronary plaque characterization, lesion-level stenosis detection, dense 3D coronary artery segmentation, and 30-day major adverse cardiac event (MACE) risk stratification. Evaluations spanned multi-center datasets from nine independent hospitals, enabling assessment of cross-site generalizability under realistic distributional shift (Fig. 1).

Conventional self-supervised learning strategies, including masked image modeling and contrastive learning, optimize for global anatomical reconstruction, implicitly prioritizing the dominant background structures that constitute the vast majority of CCTA image content. In contrast, CORA employs a synthesis-driven self-supervised paradigm: an anatomy-guided lesion synthesis engine generates realistic calcified and non-calcified plaque morphologies and inserts them into the 12,801 unlabeled CCTA pretraining volumes, explicitly biasing representation learning toward the spatially sparse vascular pathology that governs downstream clinical tasks. CORA further employs a multi-windowing input strategy that simultaneously encodes soft-tissue, contrast-enhanced lumen, and calcium window characteristics, enabling discrimination of both plaque subtypes within a single forward pass.

CORA achieves superior plaque characterization with robust cross-site generalization

Accurate characterization of coronary plaque phenotype is central to cardiovascular risk stratification, as plaque composition predicts the likelihood of future rupture and acute coronary syndrome. We fine-tuned and evaluated CORA on this task as a volume-level multi-label classification problem predicting the simultaneous presence of non-calcified and calcified plaques. Training and internal test cohorts were derived from Northwestern Memorial Hospital (N=2,220 and 555, respectively); the external test cohort comprised 2,108 patients from eight geographically and demographically distinct hospitals. The dataset characteristics used for fine-tuning are summarized in Table 1.

Across both internal and external test sets, CORA consistently outperformed all comparison methods (Fig. 2). On the internal cohort, CORA achieved AUROCs of 0.94 (95% CI: 0.92–0.96) for calcified plaque and 0.79 (95% CI: 0.75–0.83) for non-calcified plaque, substantially exceeding the baseline trained from scratch (0.74 [0.70–0.78] and 0.65 [0.60–0.70], respectively; both $p < 0.001$). CORA demonstrated consistent performance advantages over MAE, VolumeFusion, and VoCo across both plaque subtypes ($p < 0.001$), reflecting its capacity to encode the distinct attenuation signatures of each phenotype.

Performance advantages were further amplified on the external test cohort, where CORA achieved AUROCs of 0.93 (95% CI: 0.91–0.94) for calcified plaque and 0.71 (95% CI: 0.69–0.73) for non-calcified plaque. By contrast, competing methods consistently fell below 0.70 AUROC on external evaluation: MAE achieved 0.71 (95% CI: 0.68–0.73) and 0.58 (95% CI: 0.56–0.60), VolumeFusion 0.72 (95% CI: 0.70–0.74) and 0.59 (95% CI: 0.57–0.62), and VoCo 0.72 (95% CI: 0.70–0.74) and 0.61 (95% CI: 0.59–0.63) for non-calcified and calcified plaque, respectively (all comparisons vs. CORA $p < 0.0001$). These findings demonstrate that pathology-centric synthesis-driven pretraining enables CORA to learn transferable representations that are robust to site-specific imaging variability.

Table 1. Baseline demographic, clinical, and imaging characteristics of the training and validation cohorts used for coronary plaque identification and MACE risk stratification.

Characteristic	Training Set (<i>N</i> = 2,220)	Internal Test (<i>N</i> = 555)	External Test (<i>N</i> = 2,108)
Demographics			
Age (years), mean ± SD	63.1 ± 13.8	62.0 ± 14.4	63.7 ± 13.5
Female sex, <i>n</i> (%)	935(42.1%)	215(38.7%)	1,025(48.6%)
Race, <i>n</i> (%)			
White	1,438(64.8%)	338(60.9%)	1,723(81.7%)
Black or African American	349(15.7%)	103(18.6%)	126(6.0%)
Asian ^a	98(4.4%)	26(4.7%)	82(3.9%)
Other or Unknown ^b	335(15.1%)	88(15.8%)	177(8.4%)
Clinical Characteristics			
BMI (<i>kg/m</i> ²), mean ± SD	29.0 ± 7.7	29.2 ± 7.3	29.8 ± 7.2
Systolic BP (mmHg), mean ± SD	127.8 ± 19.3	127.1 ± 18.9	128.6 ± 19.7
Diastolic BP (mmHg), mean ± SD	72.4 ± 12.8	72.3 ± 12.6	73.3 ± 12.2
Tobacco Use, <i>n</i> (%)			
Never	1,041(46.9%)	255(45.9%)	1,031(48.9%)
Former	430(19.4%)	113(20.4%)	560(26.6%)
Current	114(5.1%)	27(4.9%)	136(6.5%)
Hypertension within 1 year, <i>n</i> (%)	990(44.6%)	264(47.6%)	1,062(50.4%)
Diabetes mellitus, <i>n</i> (%)	318(14.3%)	81(14.6%)	339(16.1%)
Laboratory Metrics			
Total Cholesterol (mg/dL)	170.0 ± 47.0	171.8 ± 47.1	171.0 ± 73.5
LDL Cholesterol (mg/dL)	96.5 ± 43.8	98.3 ± 37.9	93.7 ± 37.4
HDL Cholesterol (mg/dL)	49.7 ± 17.3	50.3 ± 17.5	51.9 ± 17.1
Imaging Findings			
Non-calcified Plaque present, <i>n</i> (%)	963(43.4%)	237(42.7%)	935(44.4%)
Calcified Plaque present, <i>n</i> (%)	1,300(58.6%)	326(58.7%)	1,390(65.9%)
Clinical Outcome			
30-day MACE, <i>n</i> (%)	192(8.6%)	48(8.6%)	237(11.2%)

^aIncludes Asian Indian, Chinese, Filipino, Korean, Vietnamese, Japanese, and Other Asian.

^bIncludes American Indian, Pacific Islander, Declined, and Unknown.

To investigate the interpretability of our model, we employed Grad-CAM⁴² to visualize the diagnostic signals driving the model’s predictions. As shown in Fig. 2e, the attention maps reveal that CORA consistently directs its focus to the coronary artery regions, exhibiting the highest activation levels precisely at the site of suspected plaques. For non-calcified lesions, the model’s attention aligns with low-attenuation areas along the vessel wall, even in cases with poor contrast-to-noise ratios. For calcified plaques, the activations are localized to high-intensity voxels. This targeted attention demonstrates that the model has internalized a physiologically grounded understanding of coronary anatomy and pathology, rather than relying on spurious background correlations or extra-cardiac noise.

Pathology-aware pretraining sensitizes CORA to subtle coronary stenosis

Automated lesion-level stenosis detection is essential for CAD-RADS grading and guides decisions on downstream invasive coronary angiography, yet it remains among the most challenging CCTA analysis tasks due to the morphological heterogeneity of calcified versus non-calcified plaques, the limited spatial resolution of standard CCTA acquisitions, and the absence of large curated annotated datasets. Fig. 3a illustrates the distinct morphological features of low-contrast non-calcified plaques and high-attenuation calcified lesions that often complicate automated detection.

We evaluated stenosis detection at the lesion level on 348 CCTA volumes comprising 556 annotated stenotic lesions (340 calcified, 216 non-calcified) across CAD-RADS grades 2–5 (Fig. 3b). A predicted lesion was scored as correct if it spatially overlapped with a ground-truth annotation. CORA attained an overall Precision of 0.694, Recall of 0.675, and F1-score of 0.684, compared with 0.560, 0.538, and 0.549 for the training from scratch baseline. Among 3D

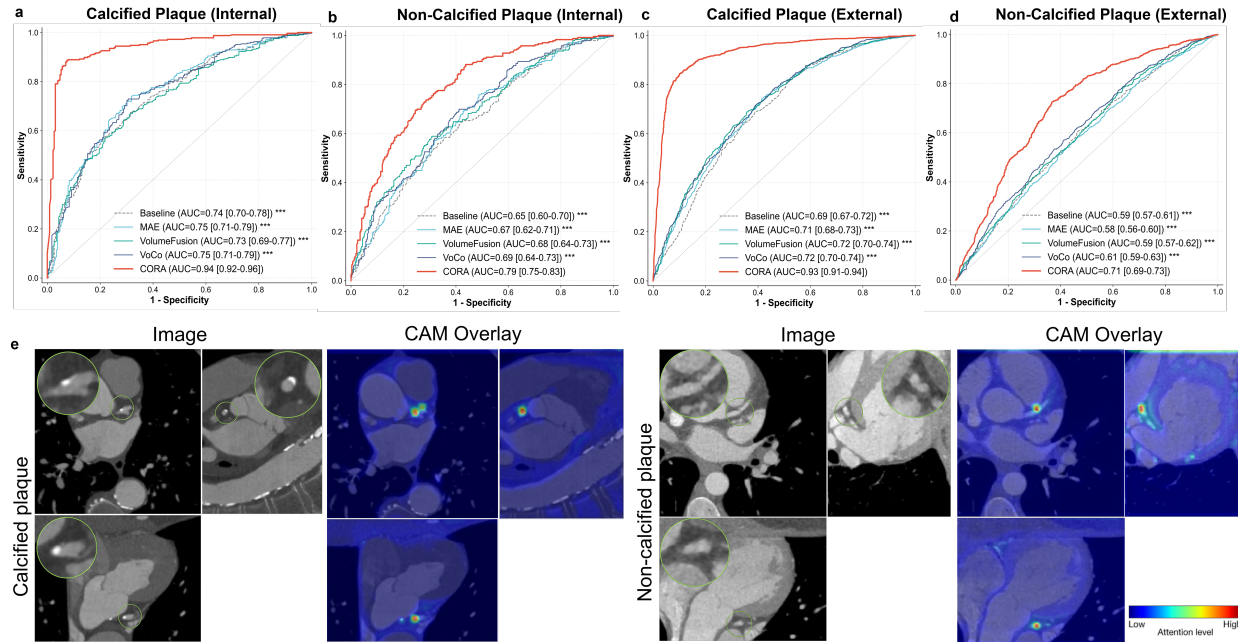


Figure 2. Performance of plaque characterization across internal and external cohorts. Receiver operating characteristic (ROC) curves for the detection of calcified and non-calcified coronary plaques on the internal test cohort (a,b) and external multi-center cohort (c,d). CORA consistently outperformed models trained from scratch and existing 3D foundation models, with the largest performance gains observed on the external cohort, indicating superior generalization under domain shift. e, Visualization of model attention using Grad-CAM showed model accurately identified plaque regions in CCTA volumes. The 95% CIs for AUCs were computed using 500 bootstrap resamples. Differences in AUCs were assessed using a bootstrap test. Statistical significance is denoted as $*p < 0.05$, $**p < 0.01$, and $***p < 0.001$.

foundation models, CORA exceeded MAE (F1=0.575; +19% relative), VolumeFusion (F1=0.550; +24%), and VoCo (F1=0.612; +12%) (Fig. 3c).

CORA improves coronary artery segmentation efficiency across data regimes

Dense 3D coronary artery segmentation provides the anatomical scaffold required for stenosis grading, fractional flow reserve estimation, and surgical planning. It remains technically demanding due to the fine vessel calibre, complex branching architecture, and low contrast of distal coronary segments. We evaluated CORA on the ImageCAS benchmark⁴³, which contains expert-annotated coronary artery masks for approximately 1,000 CCTA volumes. We reserved 40 cases for validation and 60 for testing.

In the primary evaluation using 100 labeled training samples, CORA achieved a Dice Similarity Coefficient of 0.654, Centerline Dice (cDice) of 0.681, and Mean Surface Distance (MSD) of 22.664 voxels, outperforming the baseline training from scratch across all metrics (Dice=0.629, cDice=0.651, MSD=27.264) and established 3D foundation models including MAE, VolumeFusion, and VoCo — particularly in vessel continuity as captured by cDice (Fig. 4a). The 17% reduction in MSD (22.664 vs. 27.264 voxels) reflects more accurate delineation of vessel boundaries, which is consequential for downstream quantitative lumen analysis.

We further examined data efficiency by varying the number of labeled training samples (50, 100, 200, 400, and 800). As shown in Fig. 4b, CORA consistently outperformed the baseline across all training set sizes, with particularly pronounced gains in the low-data regime. Notably, although CORA's pretraining paradigm specifically targets coronary plaque abnormalities, the pretraining significantly improved anatomical segmentation performance. This cross-task benefit suggests that pathology-aware pretraining objectives inherently refine the model's geometric understanding of vascular morphology.

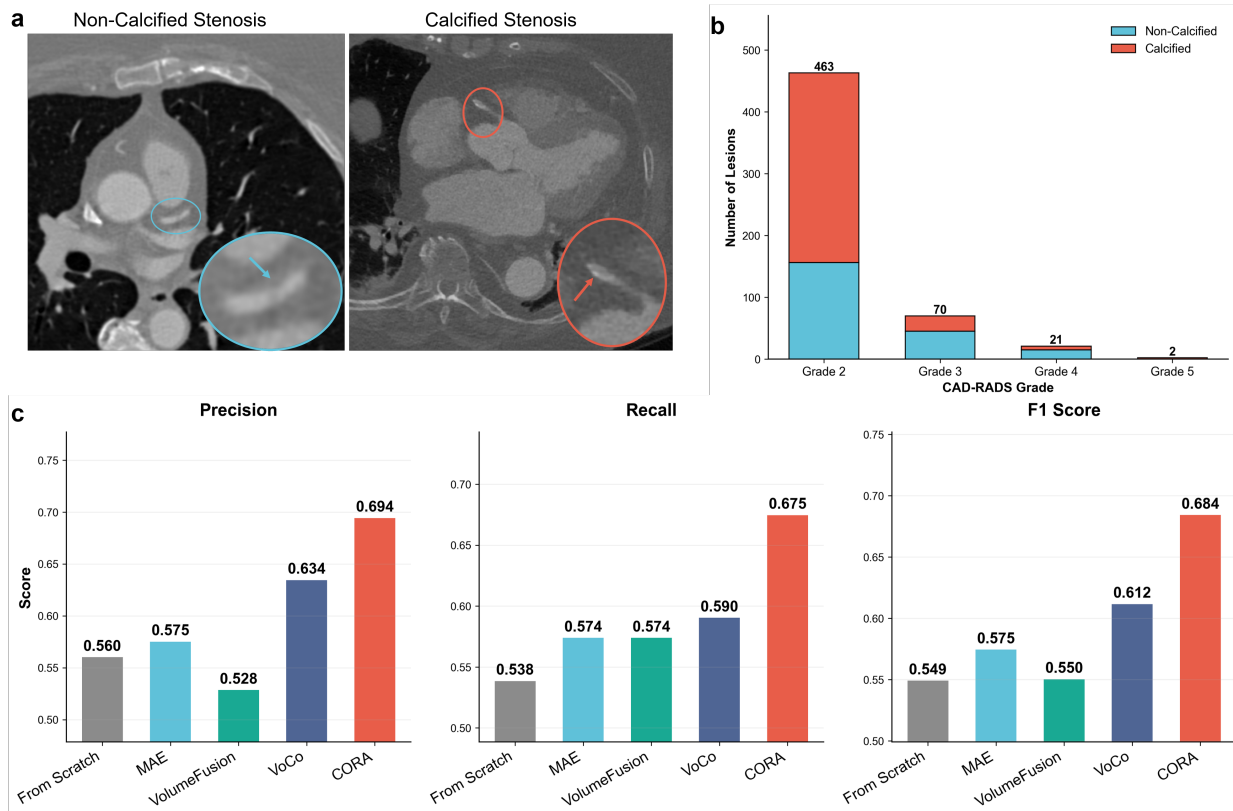


Figure 3. CORA performance in coronary stenosis detection. (a) Representative axial CCTA images illustrating the target pathologies. Magnified insets detail a low-contrast non-calcified stenosis (left, blue) and a calcified stenosis (right, red). (b) Distribution of annotated stenoses in the entire fine-tuning dataset, stratified by CAD-RADS severity grade and plaque composition (calcified, red; non-calcified, blue). (c) Quantitative benchmarking against a baseline (From Scratch) and self-supervised 3D foundation models (MAE, VolumeFusion, VoCo). CORA (red) achieves state-of-the-art performance across Precision, Recall, and F1 Score.

Multimodal CORA predicts near-term adverse cardiac events with cross-center generalizability

For patients presenting with acute chest pain, the 30-day window represents the highest-risk period for major adverse cardiac events (MACE), defined as cardiac-related mortality, myocardial infarction, or revascularization⁴⁴. Accurate early prediction of whether a patient will experience a MACE event within this acute phase carries substantial clinical value for triage, treatment planning, and resource allocation.

Given the established prognostic value of CCTA-derived plaque characteristics and clinical risk factors for major adverse cardiac event (MACE) prediction^{44–46}, we evaluated CORA for MACE prediction using the cohort described in Table 1 (training N=2,220; internal test N=555; external test N=2,108; 30-day MACE rates 8.6%, 8.6%, 11.2% respectively). Details of the study population and outcome definitions are provided in the Methods. Beyond the image-only setting, we constructed a multimodal variant of CORA that integrates CCTA-derived imaging representations with demographic and clinical variables through a frozen Qwen-7B text encoder⁴⁷. The resulting multimodal embeddings were used for 30-day MACE risk stratification. Results are summarized in Fig. 5.

On the internal test set, CORA(Multimodal) achieved the highest AUC of 0.75 (95% CI: 0.67–0.82), followed by CORA(Image) at 0.74 (95% CI: 0.65–0.81), demonstrating the incremental benefit of integrating clinical metadata alongside imaging features. Among comparison methods, VoCo attained an AUC of 0.67, while the baseline model achieved 0.64. Notably, MAE (AUC=0.62) and VolumeFusion (AUC=0.622) both fell below the baseline, demonstrating that generic self-supervised pretraining, which optimized for anatomical reconstruction rather than pathological prognosis signals, can impair prognostic performance relative to training from scratch.

On the external test set, CORA's advantage was markedly amplified. CORA(Multimodal) achieved an AUC of

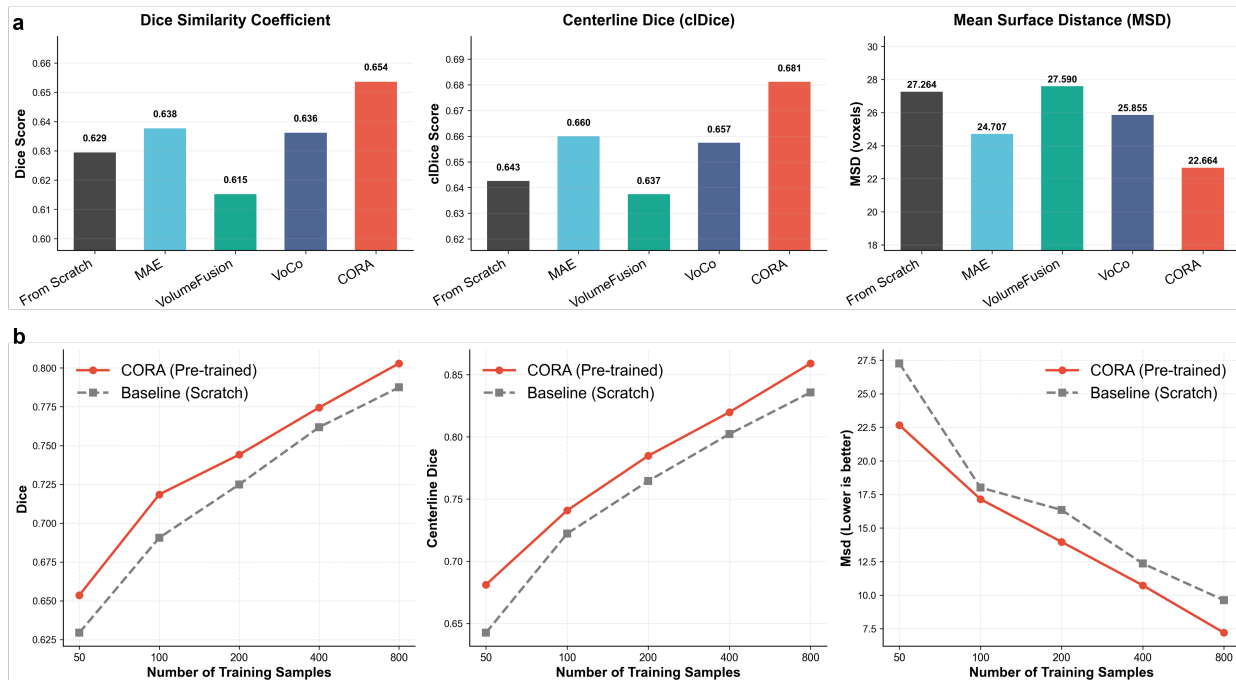


Figure 4. Coronary artery segmentation performance and data efficiency. (a) Segmentation performance on the ImageCAS test set using 100 labeled training samples, evaluated by Dice similarity coefficient, centerline Dice (cIDice), and mean surface distance (MSD). CORA outperformed models trained from scratch and existing 3D foundation models across all metrics. (b) Data efficiency analysis across varying numbers of labeled training samples (50–800). CORA consistently achieved higher segmentation accuracy and better centerline preservation than the baseline, with the largest gains observed in low-data regimes.

0.756 (95% CI: 0.722–0.789), outperforming CORA(Image) at 0.68 (95% CI: 0.64–0.72; $p < 0.001$), and substantially exceeding all competing methods: the baseline (AUC=0.59), MAE (0.59), VolumeFusion (0.57), and VoCo (0.59) — all performing near the no-information rate (all comparisons vs. CORA(Multimodal) $p < 0.001$). The multimodal fusion gain was larger externally (AUROC gain +0.08) than internally (+0.01), suggesting that clinical features contribute disproportionately to generalization across populations with heterogeneous risk profiles.

The consistent and sizeable performance gains on the external cohort, which exhibited a higher MACE event rate than the internal cohort (11.2% vs. 8.6%) and a different demographic composition, highlight the strong generalizability of CORA’s learned representations. These results demonstrate that CORA captures clinically meaningful, transferable features of coronary anatomy and plaque burden that are complementary to structured clinical risk factors in predicting near-term adverse outcomes.

Discussion

In this study, we introduced CORA, a synthesis-driven 3D vision foundation model designed for comprehensive coronary artery disease assessment and risk stratification from CCTA. By leveraging a pathology-centric self-supervised learning paradigm and large-scale unlabeled data, CORA demonstrated consistent performance gains across a diverse spectrum of downstream tasks, including plaque type characterization, lesion-level stenosis detection, coronary artery segmentation, and short-term MACE prediction. Notably, these improvements were observed not only in internal evaluations but also in independent external cohorts, underscoring the robustness and generalizability of the learned representations. Collectively, our findings suggest that pathology-aware pretraining can serve as a scalable alternative to annotation-intensive supervised learning for cardiovascular imaging.

A central contribution of this work lies in reframing representation learning from generic anatomical reconstruction toward pathology-oriented understanding. Conventional self-supervised paradigms, such as masked image modeling,

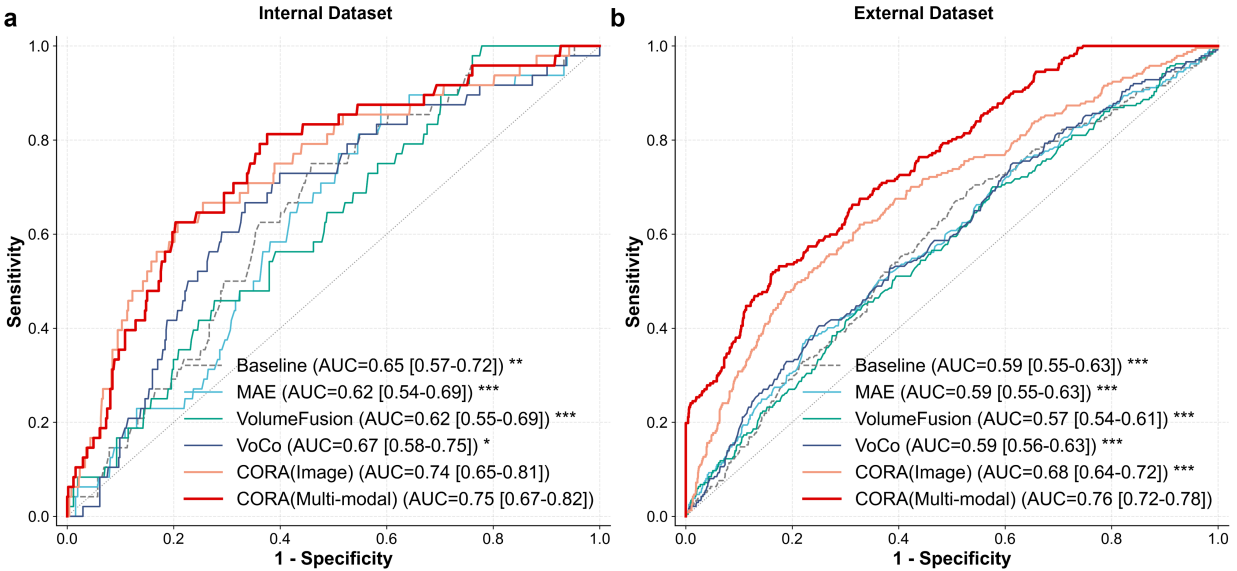


Figure 5. CORA performance in MACE prediction. Receiver operating characteristic (ROC) curves for MACE risk stratification on the internal (a) and external (b) validation datasets. The vision-only CORA(Image) (light red) consistently outperforms the supervised baseline and state-of-the-art 3D foundation models (MAE, VolumeFusion, VoCo). Fusing clinical metadata with imaging representations, CORA(Multi-modal) (solid red) achieves the highest prognostic accuracy and robust cross-center generalization. The 95% CIs for AUCs were computed using 500 bootstrap resamples. Differences in AUCs were assessed using a bootstrap test. Statistical significance is denoted as $*p < 0.05$, $**p < 0.01$, and $***p < 0.001$.

implicitly emphasize global anatomical statistics and reconstruction fidelity. While effective for structural tasks, these objectives may dilute the representation of spatially sparse pathological signals, particularly in CCTA where coronary plaques occupy only a small fraction of the volumetric field of view. In contrast, the synthesis-driven objective adopted in CORA explicitly biases the encoder toward detecting simulated vascular abnormalities. This formulation encourages the model to allocate representational capacity to subtle, localized intensity and morphological variations that characterize plaque phenotypes. Furthermore, the multi-windowing input strategy enables simultaneous exploitation of complementary attenuation ranges, facilitating improved discrimination between low-attenuation non-calcified plaques and high-density calcified lesions. The consistent gains observed across both diagnostic and anatomical tasks suggest that pathology-centric objectives can simultaneously enhance disease sensitivity and structural awareness.

Compared with existing 3D foundation models and task-specific baselines, CORA demonstrated superior cross-domain generalization, with the largest performance margins observed on external datasets. This finding highlights an important limitation of conventional self-supervised approaches in medical imaging: features learned through generic reconstruction objectives may remain entangled with scanner- or protocol-specific characteristics, limiting transferability across institutions. By contrast, lesion synthesis introduces task-relevant invariances, enabling the model to focus on physiologically meaningful patterns that are less sensitive to acquisition variability. Additionally, the unified encoder architecture supports multiple downstream tasks without reliance on complex multi-stage pipelines, potentially reducing cumulative error propagation associated with vessel extraction and reformatting workflows.

An important consideration concerns the fidelity of synthetic lesions relative to the full biological complexity of atherosclerotic plaques. Real-world coronary lesions exhibit a rich spectrum of morphological and compositional heterogeneity that cannot be exhaustively captured by any simulation engine, including lipid-rich necrotic cores, fibrous caps of variable thickness, spotty calcification, and napkin-ring signs. However, we emphasize that perfect pathological realism is neither the design goal nor a prerequisite for effective pretraining. The synthesis engine serves a specific representational purpose: to redirect the encoder’s attention from dominant background anatomy toward the coronary vasculature and its potential abnormalities, thereby reducing the learning burden during subsequent task-specific fine-tuning. From this perspective, the critical property of synthetic lesions is not biological fidelity but rather morphological

and attenuation diversity, ensuring that the pretrained encoder develops broad sensitivity to a wide range of intensity perturbations along the vessel wall. Empirically, when we applied the pretrained model directly to real CCTA volumes without any fine-tuning (Fig. S3), the resulting abnormality response maps highlighted numerous candidate regions, with genuine lesions consistently included among them. Although these raw predictions also contained substantial false positives, this behavior is expected and, in fact, desirable: it indicates that the pretrained encoder has acquired a deliberately over-sensitive detector that casts a wide net over plaque-like regions. Task-specific fine-tuning then refines this broad sensitivity into precise, clinically actionable predictions by leveraging labeled examples to suppress false positives and sharpen lesion discrimination.

Furthermore, a notable property of our pretraining framework is its complete independence from diagnostic labels. Because the supervisory signal derives entirely from synthetically inserted lesions, CORA can be pretrained on any CCTA volume regardless of whether the patient harbors genuine coronary atherosclerosis. In practice, a subset of the 12,801 pretraining volumes inevitably contains real plaques that are not labeled as positive targets during pretraining. However, several design properties mitigate the impact of this implicit label noise. The patch-based sampling strategy ($96 \times 96 \times 96$ voxels) ensures that the vast majority of randomly cropped patches do not intersect with real coronary plaques, given their well-established spatial sparsity within the volumetric scan. Furthermore, the large batch size and dataset scale ensure that any noisy gradients from such patches are highly diluted across training iterations. The strong downstream performance across all evaluated tasks provides empirical confirmation that this noise does not meaningfully impair representation quality. More broadly, this property makes the pretraining pipeline immediately scalable to any institutional CCTA archive without curation overhead.

From a clinical perspective, these results have several implications. First, accurate plaque characterization and stenosis detection are critical for diagnostic and therapeutic decision-making in patients with suspected coronary artery disease. The improved sensitivity and robustness of CORA may facilitate automated screening and prioritization of high-risk studies, thereby reducing interpretation time and inter-observer variability. Second, the multimodal extension integrating demographic and clinical information yielded improved MACE prediction, suggesting that imaging-derived representations capture prognostically relevant features beyond traditional clinical risk factors. Such integration could support early triage in acute chest pain settings and enable more personalized management strategies. Finally, the unified nature of the proposed foundation model may provide a practical pathway toward scalable deployment across heterogeneous clinical environments.

Several limitations of the current work warrant acknowledgment. First, the clinical composition of our dataset inherently limits the generalizability of the model to asymptomatic populations. In routine clinical practice, CCTAs are primarily acquired for patients with specific clinical indications, most commonly symptomatic chest pain or anginal equivalents. Consequently, the generalizability of CORA to asymptomatic screening populations cannot be assumed without dedicated evaluation. The atherosclerotic burden, plaque morphology distribution, and pretest probability in such cohorts may differ substantially from the symptomatic populations represented in our training and validation data. Future prospective studies should assess model performance in asymptomatic individuals undergoing CCTA as part of emerging primary prevention protocols. Second, our evaluation was based on a retrospective study design, which may not capture the full clinical context of a prospective longitudinal follow-up. Consequently, the labels for 30-day MACE may contain a degree of noise; for instance, out-of-hospital cardiac-related mortality or events occurring at external institutions might not be fully captured within our integrated healthcare system's records. While the probability of such missing events within a narrow 30-day window is relatively low, this potential for under-reporting remains a factor. Future prospective studies with dedicated event adjudication are necessary to further validate these prognostic findings. Third, our dataset lacked comprehensive baseline data regarding concurrent lipid-lowering therapies (e.g., statin medications). Statins are known to modify plaque biology, often promoting macroscopic calcification while reducing non-calcified lipid cores to stabilize plaques. While the absence of this pharmacological context is a limitation, the strong prognostic performance of CORA across both internal and external cohorts, regardless of underlying medication status, underscores the robustness and broad generalizability of the learned representations in real-world, highly heterogeneous clinical settings.

In conclusion, CORA demonstrates that pathology-centric synthesis-driven pretraining provides an effective strategy for learning clinically meaningful representations from large-scale unlabeled CCTA data. By unifying anatomical assessment and prognostic modeling within a single foundation framework, this approach offers a scalable pathway toward comprehensive, data-efficient cardiovascular imaging analysis.

Methods

Study population

We retrospectively analyzed a cohort of 12,801 patients who underwent CCTA between October 2005 and November 2024 across nine hospitals within the Northwestern Medicine healthcare system. The study was approved by the Institutional Review Board of Northwestern University, with a waiver for informed consent. Clinical indications for CCTA included symptomatic chest pain, risk-factor-based screening for coronary artery disease (CAD), electrocardiographic abnormalities, or evaluation of prior revascularization. CCTA examinations were performed using a 64-detector row or higher single- or dual-source CT scanner (Somatom Force or Somatom Definition Flash, Siemens Healthineers; Revolution CT or Revolution Apex, GE HealthCare; Aquilion Prime 80, Canon Medical Systems). All CCTA volumes were identified for analysis. All the CCTA volume in pretraining and fine-tuning phase were resampled to a fixed voxel spacing of $0.5 \times 0.5 \times 5 \text{ mm}^3$.

To establish the dataset for plaque characterization and MACE prediction, we applied the following exclusion criteria: 1) History of coronary revascularization. 2) Coronary artery bypass graft surgery. 3) Prior acute myocardial infarction. 4) Absence of follow-up diagnostic records following the index CCTA. The final study population consisted of 4,883 eligible subjects with an average follow-up of 2.4 years. Of these, 2,775 patients were from Northwestern Memorial Hospital, partitioned into a training set ($N = 2,220$) and an internal validation set ($N = 555$). The remaining 2,108 patients from the other eight hospitals were reserved as an independent external validation cohort. The demographic, clinical, and imaging characteristics for each cohort are summarized in Table 1. The detailed inclusion and exclusion process, including patient partitioning across the nine participating centers, is illustrated in the study flow diagram (Fig. S1). Plaque classification labels were systematically extracted from the original CCTA radiology reports to provide ground-truth annotations for model training and validation.

The dataset for stenosis detection was established as a subset of the cohort described above. We identified 348 CCTA volumes that contained at least one lesion with mild or greater severity (CAD-RADS ≥ 2), as indicated in the original clinical radiology reports. To ensure diagnostic-grade ground truth, three experienced radiologists and medical imaging experts independently annotated the stenotic lesions, using the corresponding radiology reports as a primary reference for localization and grading.

CORA implementation and pretraining protocol

We framed the pretraining of CORA as a self-supervised segmentation task, utilizing a 3D Residual U-Net architecture (Table S1). To prioritize the learning of clinically relevant features, we developed a "pathology-aware" data engine that performs real-the-fly synthesis of coronary abnormalities within the vascular tree. This strategy biases the model's representational capacity toward the coronary vasculature and its associated pathologies, rather than generic anatomical reconstruction.

Table S1. Architectural specifications of the CORA model during the pretraining. The network follows a 3D Residual U-Net design with a four-stage encoder-decoder structure.

Part	Stage	Operation	Output Features	Stride	Blocks
Input	-	CCTA Multi-channel Patch	4×96^3	-	-
Encoder	Stage 1	3D ResBlock	32×96^3	[1, 1, 1]	1
	Stage 2	3D ResBlock	64×48^3	[2, 2, 2]	3
	Stage 3	3D ResBlock	128×24^3	[2, 2, 2]	4
	Stage 4	3D ResBlock (Bottleneck)	256×12^3	[2, 2, 2]	4
Decoder	Stage 3	Upsampling + 3D Conv	128×24^3	[2, 2, 2]	1
	Stage 2	Upsampling + 3D Conv	64×48^3	[2, 2, 2]	1
	Stage 1	Upsampling + 3D Conv	32×96^3	[2, 2, 2]	1
Output	-	$1 \times 1 \times 1$ Convolution	1×96^3	-	Sigmoid

Note: All convolutional layers use $3 \times 3 \times 3$ kernels followed by Instance Normalization and LeakyReLU.

Data engine To facilitate the data engine, we first extracted coronary artery masks from the pretraining volumes using a nn-unet⁴⁸ model trained on the ImageCAS dataset⁴³. During the pretraining, an artery-centric sampling strategy: patches of size $64 \times 64 \times 64$ were randomly cropped, with the center of each patch anchored to a coronary artery

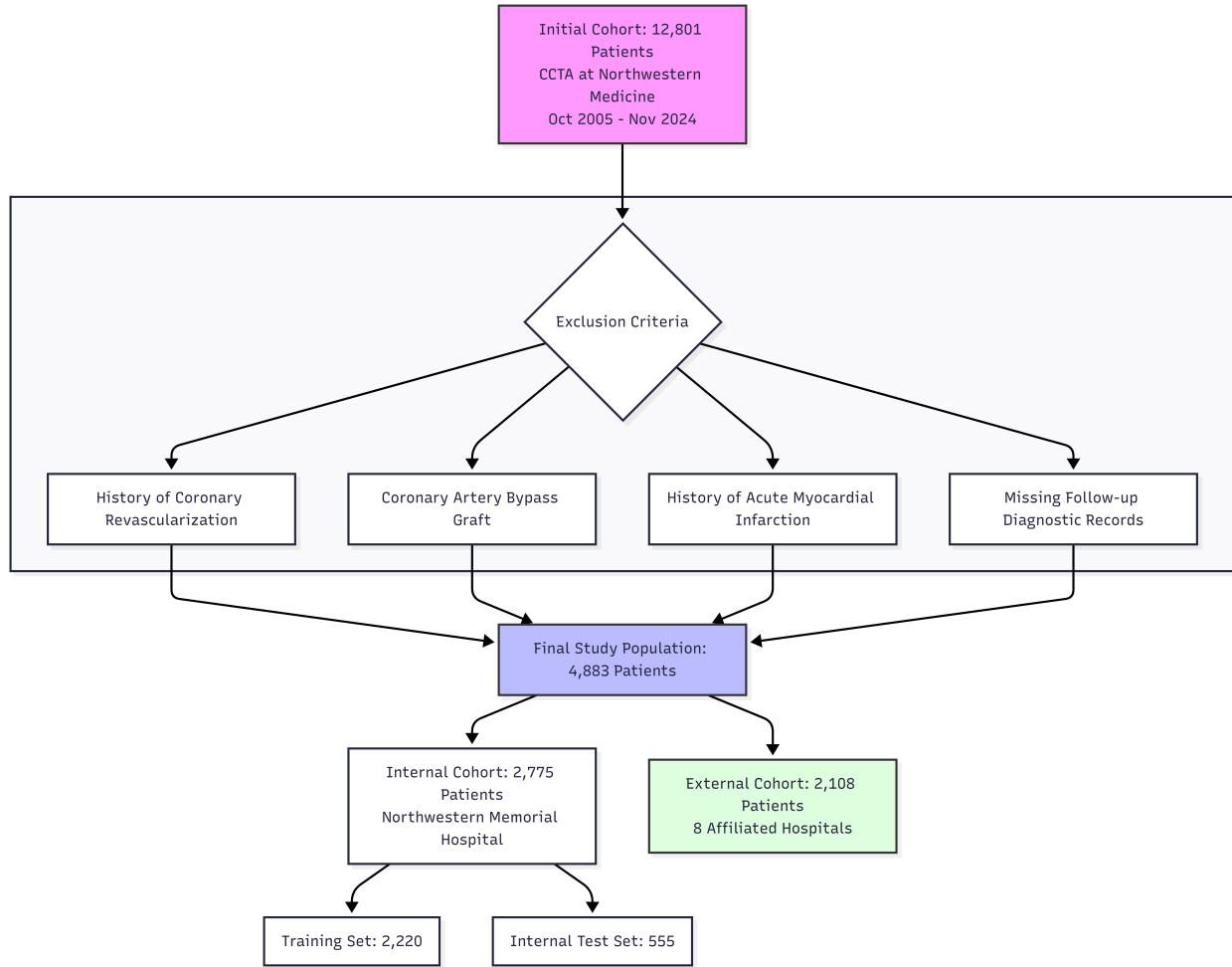


Figure S1. Flowchart of study population selection and cohort partitioning that used in plaque characterization and MACE prediction tasks. From an initial cohort of 12,801 patients, 4,883 were included after excluding those with prior revascularization, myocardial infarction, or missing follow-up. The final population was partitioned into an internal development cohort ($N = 2,775$; split 80/20 for training and testing) and an independent external validation cohort ($N = 2,108$) across nine hospitals.

voxel. This ensures that every training sample contains valid vascular anatomy, maximizing the learning signal for coronary-specific features.

Within each vascular patch, we stochastically inserted synthetic calcified or non-calcified (soft) plaques. We utilized a data engine to generate irregular, realistic lesion morphologies. Lesions were modeled as composite structures formed by 1–3 overlapping Gaussian blobs (sigma range: 0.7 – 2.0) to simulate the heterogeneous shapes of natural plaques. Synthetic lesions were assigned Hounsfield Unit (HU) values according to their clinical phenotype: 800 – 1500 HU for calcified plaques and 30 – 90 HU for soft plaques. To provide the model with enhanced contrast sensitivity, the raw patch was transformed into a four-channel input using specific clinical windows: Fat Window (–100, 140 HU), Soft tissue Window (50, 400 HU), Angiographic Window (350, 700 HU) and Calcification Window (500, 2000 HU). To enhance robustness and simulate clinical imaging conditions, we applied Poisson noise using a Beer-Lambert law approximation ($I_0 = 10^5$, $L = 200.0$ mm), alongside electronic background noise ($\sigma_e = 2.0$). Geometric augmentations included random 3D rotations ($\pm 15^\circ$), isotropic zooming (0.9 – 1.1), and random axis flipping. Fig. S2 provides the comparative visualization of real and synthetic coronary plaques.

Model pretraining Given that coronary lesions are highly sparse relative to the total volume, we utilized a custom loss function to address extreme class imbalance. The objective function is defined as the sum of two components: 1)

Tversky Loss⁴⁹: We set $\beta = 0.9$ and $\alpha = 0.1$ to heavily penalize false negatives, thereby prioritizing recall (sensitivity) in detecting subtle lesions. 2) Focal Loss⁵⁰: A focusing parameter of $\gamma = 4.0$ was employed to down-weight the loss contribution from easy background voxels, forcing the model to concentrate on the challenging pathological boundaries. The total loss is:

$$L_{total} = L_{Tversky}(\alpha = 0.1, \beta = 0.9) + L_{Focal}(\gamma = 4.0)$$

This synthesis-driven pretraining biases the encoder toward clinically relevant vascular pathology, providing a robust foundation for downstream diagnostic and prognostic tasks. In Fig. S3, we provided the zero-shot abnormality detection by the pretrained CORA on real CCTA volumes without any task-specific fine-tuning.

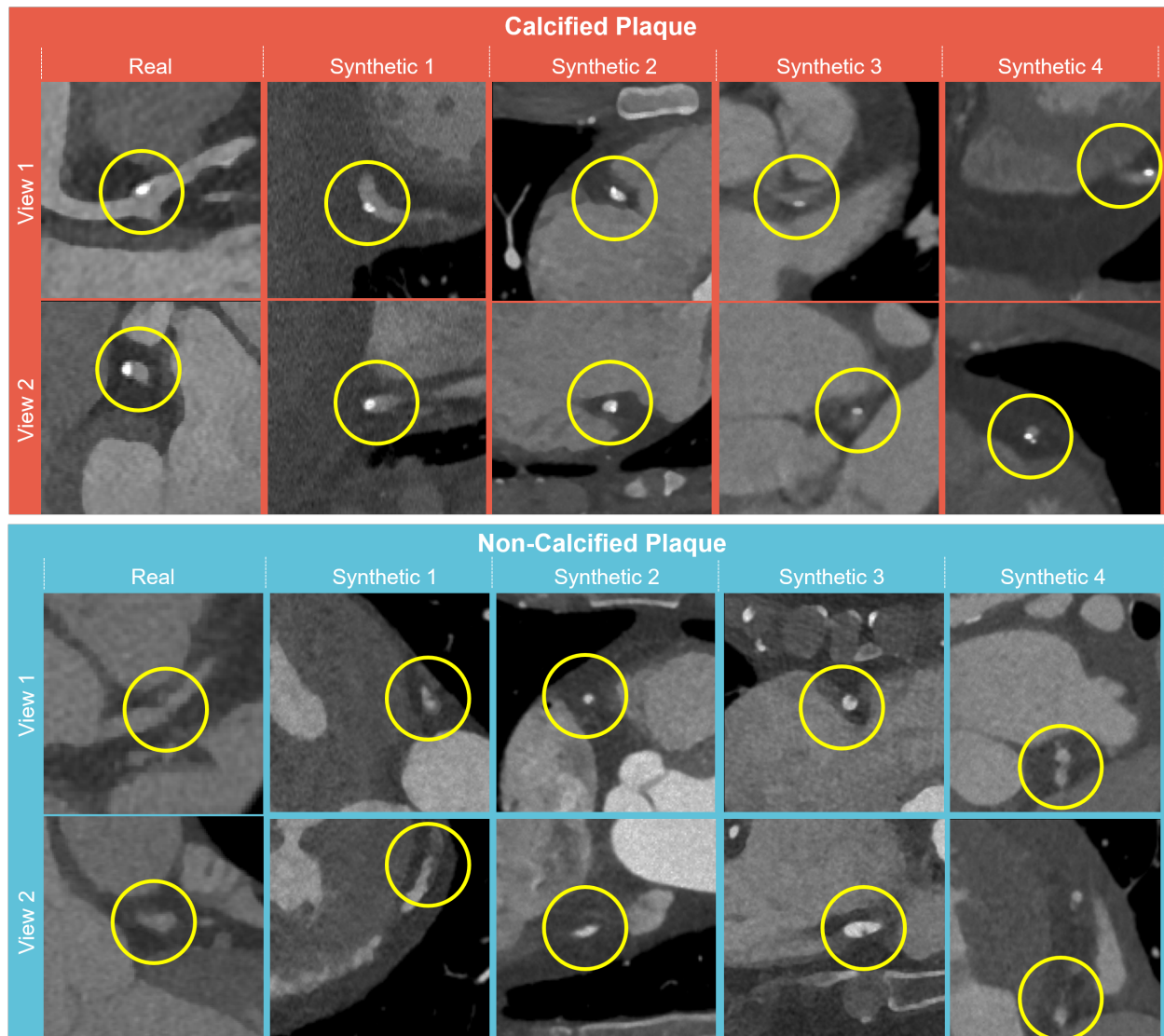


Figure S2. Comparative visualization of real and synthetic coronary plaques. Representative CCTA patches showing calcified and non-calcified plaques from the clinical dataset. Corresponding examples of synthetic calcified and non-calcified lesions generated by the CORA pathology-aware data engine. The synthetic plaques exhibit a diverse range of morphological structures and Hounsfield Unit (HU) distributions, closely mimicking the attenuation profiles and irregular geometries observed in the real-world clinical cohort.

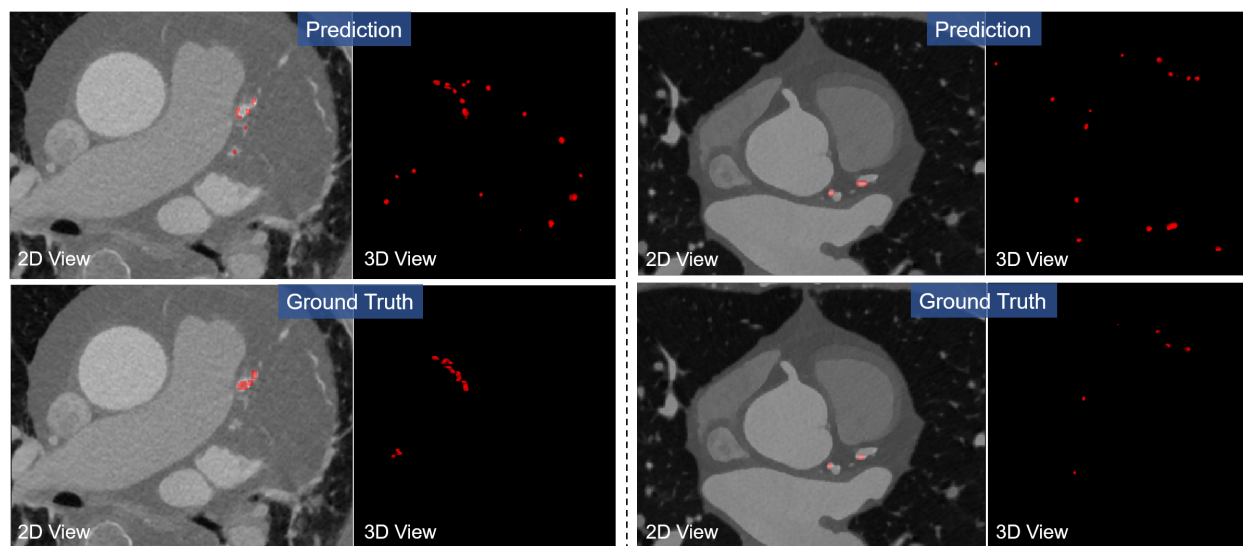


Figure S3. Anatomical attention prior established by synthesis-driven pretraining. Direct inference on real CCTA volumes using the frozen, pretrained CORA model, prior to any task-specific fine-tuning. Raw abnormality predictions (top) are compared to expert-annotated ground truth plaques (bottom) in both 2D axial and 3D spatial views. The pretrained model successfully highlights a broad set of suspected candidate regions (red). Crucially, while this raw output includes false positives, the true clinical lesions are consistently localized within these candidate sets. This demonstrates how pretraining sensitizes the encoder to "lesion-like" features, establishing a highly sensitive prior that significantly narrows the search space for downstream fine-tuning.

Adaptation to downstream tasks

Coronary plaque characterization task The coronary plaque characterization task was formulated as a volume-level multi-label classification problem to predict the presence of calcified and non-calcified plaques from CCTA volumes. During fine-tuning, we used the pretrained encoder of CORA as the backbone, followed by a global average pooling layer and a linear classification head. As this task operates at the volume level, the entire CCTA volume was used as input without patch sampling. Model performance was primarily evaluated using the area under the receiver operating characteristic curve (AUROC), as reported in the main text. In addition, we reported accuracy, sensitivity, specificity, and F1-score for both calcified and non-calcified plaque detection (Fig. S4). More class activation map visualizations are provided in Fig. S5.

Stenosis detection The stenosis detection task was formulated as a segmentation problem. For fine-tuning, both the pretrained encoder and decoder of CORA were used as initialization. To address severe class imbalance between stenotic lesions and background, we adopted a composite loss function consisting of Tversky loss and focal loss. To reduce false-positive detections and improve computational efficiency during the fine-tuning stage, we utilized TotalSegmentator⁵¹ to generate an anatomical mask of the heart. This mask was then used to crop the original CCTA volumes, effectively isolating the cardiac region and restricting the model's input to clinically relevant voxels. This preprocessing step significantly suppressed potential artifacts from extracardiac structures. Because stenosis boundaries—especially those caused by non-calcified plaques—are often ambiguous, and clinical decision-making primarily requires lesion localization rather than precise voxel-level delineation, evaluation was conducted at the lesion level. Each stenosis was defined as a connected component in the ground-truth annotation. A predicted lesion was considered a true positive if it overlapped with a reference lesion by more than 10 voxels.

Coronary artery segmentation To evaluate the transferability of our pre-trained representations to dense anatomical tasks, we fine-tuned CORA for coronary artery segmentation. In this configuration, we utilized the pre-trained CORA encoder paired with a randomly initialized decoder. The model was optimized using Dice loss to ensure overlap maximization between the predicted and reference vascular masks. This task specifically tested whether pathology-centric pretraining preserves the underlying anatomical grounding of the coronary tree.

MACE risk stratification For 30-day MACE prediction, we constructed a multimodal model integrating imaging

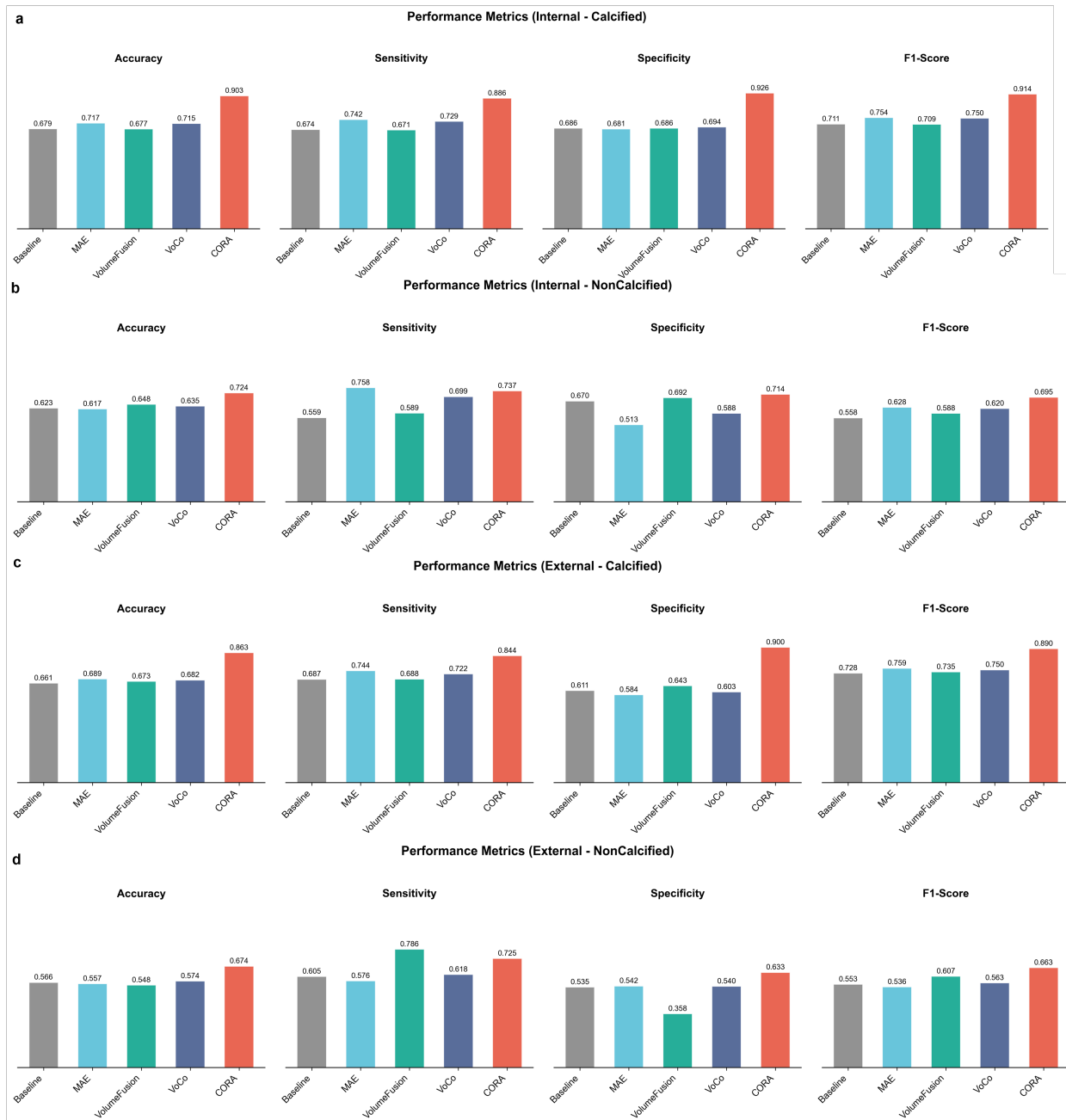


Figure S4. Detailed quantitative results of coronary plaque characterization task.

and clinical information. The pretrained CORA encoder was used as the image encoder, followed by a global average pooling layer to obtain a fixed-length representation. A frozen Qwen-7B text encoder was used to encode demographic and clinical variables listed in Table 1. These variables were formatted as natural language inputs.

To better leverage the language model’s capacity, we prepended the following prompt to the input text: “*The following is a summary of the patient’s demographic and clinical information. Please focus on key risk factors for major adverse cardiovascular events.*” The text embeddings were further projected through a multilayer perceptron (MLP) to reduce dimensionality. The image and text features were concatenated and fed into a linear classification layer for final prediction. The model was optimized using cross-entropy loss.

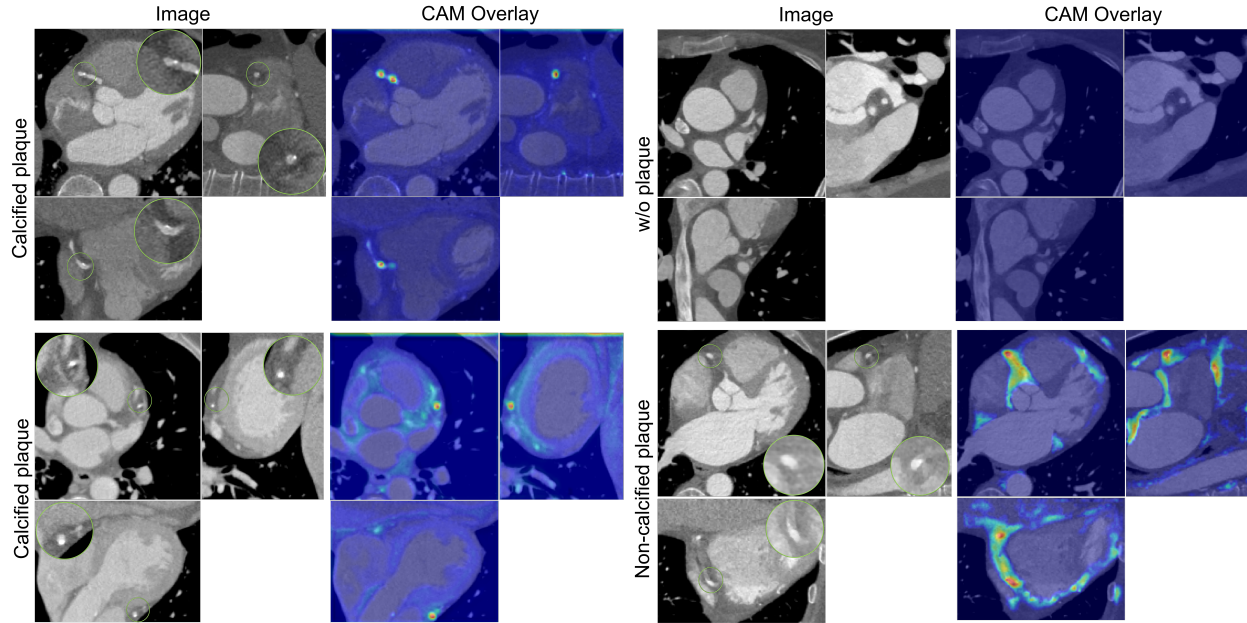


Figure S5. Grad-cam visualization of coronary plaque characterization task.

Computational resources

All model training and evaluations were performed on the Northwestern University Quest High-Performance Computing (HPC) cluster. The pretraining phase of CORA was conducted using a single NVIDIA H100 GPU (80 GB). Due to the efficient patch-based sampling strategy ($96 \times 96 \times 96$ voxels), the pretraining process was completed in approximately 25 hours. For downstream fine-tuning tasks, the computational requirements varied based on input dimensionality and dataset scale. Plaque Classification and MACE Risk Stratification: Because these tasks required processing the entire CCTA volume as input, we utilized a multi-GPU configuration consisting of three NVIDIA H100 GPUs. Training for these tasks was completed in approximately 48 hours. Coronary Artery Segmentation and Stenosis Detection: These tasks were computationally less intensive due to the smaller dataset sizes. Fine-tuning for these objectives was performed on a single NVIDIA H100 GPU, with each task reaching convergence in less than 10 hours. All implementations were developed using the PyTorch framework, leveraging specialized libraries such as SimpleITK and MONAI for medical image processing and data augmentation.

Data availability

The ImageCAS dataset was used for the evaluation of coronary artery segmentation and is publicly available at [GitHub repository](#). The datasets used for pretraining CORA, as well as for fine-tuning on the coronary plaque characterization task, stenosis detection task, and MACE risk stratification task, are not publicly available due to patient privacy obligations, Institutional Review Board (IRB) restrictions, and data use agreement requirements. De-identified data may be made available for research purposes from the corresponding authors upon reasonable request, subject to institutional approval.

Code availability

All algorithms used in this study were developed using libraries and scripts in PyTorch. The source code will be publicly available at: [\[CORA\]](#).

Author contributions statement

J.H. proposed the methodology, designed and performed all experiments, conducted the data analysis, and drafted the manuscript. G.D. and H.E.A. performed the data annotation and verified the integrity of the clinical datasets. B.Z.

conceptualized and supervised the research project. U.B., B.D.A., and N.S.S. provided critical clinical and technical insights. All authors contributed substantially to the critical revision of the manuscript for important intellectual content, and all authors reviewed and approved the final version.

Competing interests

The authors declare no competing interests.

References

1. Lindstrom, M. *et al.* Global burden of cardiovascular diseases and risks collaboration, 1990-2021. *J. Am. Coll. Cardiol.* **80**, 2372–2425 (2022).
2. Members, W. C. *et al.* 2021 aha/acc/ase/chest/saem/scct/scmr guideline for the evaluation and diagnosis of chest pain: a report of the american college of cardiology/american heart association joint committee on clinical practice guidelines. *J. Am. Coll. Cardiol.* **78**, e187–e285 (2021).
3. Narula, J. *et al.* Prospective deep learning–based quantitative assessment of coronary plaque by computed tomography angiography compared with intravascular ultrasound: the revealplaque study. *Eur. Hear. Journal-Cardiovascular Imaging* **25**, 1287–1295 (2024).
4. Jukema, R. A. *et al.* Diagnostic accuracy of non-invasive cardiac imaging modalities in patients with a history of coronary artery disease: a meta-analysis. *Heart* **111**, 4–10 (2025).
5. Williams, M. C. *et al.* Low-attenuation noncalcified plaque on coronary computed tomography angiography predicts myocardial infarction: results from the multicenter scot-heart trial (scottish computed tomography of the heart). *Circulation* **141**, 1452–1462 (2020).
6. Feuchtner, G. M. *et al.* Ai-quantitative ct coronary plaque features associate with a higher relative risk in women: Confirm2 registry. *Circ. Cardiovasc. Imaging* **18**, e018235 (2025).
7. Investigators, S.-H. Coronary ct angiography and 5-year risk of myocardial infarction. *New Engl. J. Medicine* **379**, 924–933 (2018).
8. Douglas, P. S. *et al.* Outcomes of anatomical versus functional testing for coronary artery disease. *New Engl. J. Medicine* **372**, 1291–1300 (2015).
9. Lin, A. *et al.* Deep learning-enabled coronary ct angiography for plaque and stenosis quantification and cardiac risk prediction: an international multicentre study. *The Lancet Digit. Heal.* **4**, e256–e265 (2022).
10. Thomsen, C. & Abdulla, J. Characteristics of high-risk coronary plaques identified by computed tomographic angiography and associated prognosis: a systematic review and meta-analysis. *Eur. Hear. Journal-Cardiovascular Imaging* **17**, 120–129 (2016).
11. Nurmohamed, N. S. *et al.* Development and validation of a quantitative coronary ct angiography model for diagnosis of vessel-specific coronary ischemia. *Cardiovasc. Imaging* **17**, 894–906 (2024).
12. Pinna, A. *et al.* Machine learning for coronary plaque characterization: A multimodal review of oct, ivus, and ccta. *Diagnostics* **15**, 1822 (2025).
13. Shrivastava, P. *et al.* A systematic review on deep learning-enabled coronary ct angiography for plaque and stenosis quantification and cardiac risk prediction. *Eur. J. Radiol. Open* **14**, 100652 (2025).
14. Maurovich-Horvat, P., Ferencik, M., Voros, S., Merkely, B. & Hoffmann, U. Comprehensive plaque assessment by coronary ct angiography. *Nat. Rev. Cardiol.* **11**, 390–402 (2014).
15. Ma, X., Luo, G., Wang, W. & Wang, K. Transformer network for significant stenosis detection in ccta of coronary arteries. In *International Conference on Medical Image Computing and Computer-Assisted Intervention*, 516–525 (Springer, 2021).
16. Lee, S.-E. *et al.* Differences in progression to obstructive lesions per high-risk plaque features and plaque volumes with ccta. *Cardiovasc. imaging* **13**, 1409–1417 (2020).
17. Denzinger, F. *et al.* Coronary artery plaque characterization from ccta scans using deep learning and radiomics. In *International Conference on Medical Image Computing and Computer-Assisted Intervention*, 593–601 (Springer, 2019).

18. Lorenzatti, D. *et al.* Interaction between risk factors, coronary calcium, and ccta plaque characteristics in patients aged 18–45 years. *Eur. Hear. Journal-Cardiovascular Imaging* **25**, 1071–1082 (2024).
19. Dey, D. *et al.* Automated three-dimensional quantification of noncalcified coronary plaque from coronary ct angiography: comparison with intravascular us. *Radiology* **257**, 516–522 (2010).
20. Zreik, M. *et al.* A recurrent cnn for automatic detection and classification of coronary artery plaque and stenosis in coronary ct angiography. *IEEE transactions on medical imaging* **38**, 1588–1598 (2018).
21. Du, T. *et al.* Training and validation of a deep learning architecture for the automatic analysis of coronary angiography: Automatic recognition of coronary angiography. *EuroIntervention* **17**, 32 (2021).
22. Jukema, R. A. *et al.* Artificial intelligence–based coronary plaque quantification using coronary ct angiography: Current insights and future directions. *Radiol. Cardiothorac. Imaging* **7**, e240568 (2025).
23. Ihdahid, A. R. *et al.* Coronary artery stenosis and high-risk plaque assessed with an unsupervised fully automated deep learning technique. *JACC: Adv.* **3**, 100861 (2024).
24. Gui, J. *et al.* A survey on self-supervised learning: Algorithms, applications, and future trends. *IEEE Transactions on Pattern Analysis Mach. Intell.* **46**, 9052–9071 (2024).
25. Zhang, S. & Metaxas, D. On the challenges and perspectives of foundation models for medical image analysis. *Med. image analysis* **91**, 102996 (2024).
26. Awais, M. *et al.* Foundation models defining a new era in vision: a survey and outlook. *IEEE Transactions on Pattern Analysis Mach. Intell.* **47**, 2245–2264 (2025).
27. Zhou, Y. *et al.* A foundation model for generalizable disease detection from retinal images. *Nature* **622**, 156–163 (2023).
28. Chen, R. J. *et al.* Towards a general-purpose foundation model for computational pathology. *Nat. medicine* **30**, 850–862 (2024).
29. Wang, X. *et al.* A pathology foundation model for cancer diagnosis and prognosis prediction. *Nature* **634**, 970–978 (2024).
30. Ma, C., Tan, W., He, R. & Yan, B. Pretraining a foundation model for generalizable fluorescence microscopy-based image restoration. *Nat. Methods* **21**, 1558–1567 (2024).
31. Tejada-Lapuerta, A. *et al.* Nicheformer: a foundation model for single-cell and spatial omics. *Nat. methods* 1–14 (2025).
32. Yao, J. *et al.* Eva-x: A foundation model for general chest x-ray analysis with self-supervised learning. *npj Digit. Medicine* **8**, 678 (2025).
33. Zhou, Z., Sodha, V., Pang, J., Gotway, M. B. & Liang, J. Models genesis. *Med. image analysis* **67**, 101840 (2021).
34. Chen, Z. *et al.* Masked image modeling advances 3d medical image analysis. In *Proceedings of the IEEE/CVF Winter Conference on Applications of Computer Vision*, 1970–1980 (2023).
35. Yan, K. *et al.* Sam: Self-supervised learning of pixel-wise anatomical embeddings in radiological images. *IEEE Transactions on Med. Imaging* **41**, 2658–2669 (2022).
36. Wald, T. *et al.* Revisiting mae pre-training for 3d medical image segmentation. In *Proceedings of the Computer Vision and Pattern Recognition Conference*, 5186–5196 (2025).
37. Wang, H. *et al.* Sam-med3d: A vision foundation model for general-purpose segmentation on volumetric medical images. *IEEE Transactions on Neural Networks Learn. Syst.* (2025).
38. Wald, T. *et al.* An openmind for 3d medical vision self-supervised learning. In *Proceedings of the IEEE/CVF International Conference on Computer Vision*, 23839–23879 (2025).
39. He, K. *et al.* Masked autoencoders are scalable vision learners. In *Proceedings of the IEEE/CVF conference on computer vision and pattern recognition*, 16000–16009 (2022).
40. Wang, G. *et al.* Mis-fm: 3d medical image segmentation using foundation models pretrained on a large-scale unannotated dataset. *arXiv preprint arXiv:2306.16925* (2023).
41. Wu, L., Zhuang, J. & Chen, H. Large-scale 3d medical image pre-training with geometric context priors. *IEEE Transactions on Pattern Analysis Mach. Intell.* (2025).

42. Selvaraju, R. R. *et al.* Grad-cam: Visual explanations from deep networks via gradient-based localization. In *Proceedings of the IEEE international conference on computer vision*, 618–626 (2017).
43. Zeng, A. *et al.* Imagecas: A large-scale dataset and benchmark for coronary artery segmentation based on computed tomography angiography images. *Comput. Med. Imaging Graph.* **109**, 102287 (2023).
44. Schlett, C. L. *et al.* Prognostic value of ct angiography for major adverse cardiac events in patients with acute chest pain from the emergency department: 2-year outcomes of the romicat trial. *JACC: Cardiovasc. Imaging* **4**, 481–491 (2011).
45. Hou, Z.-h. *et al.* Prognostic value of coronary ct angiography and calcium score for major adverse cardiac events in outpatients. *JACC: Cardiovasc. Imaging* **5**, 990–999 (2012).
46. Kolossváry, M. *et al.* Coronary plaque radiomic phenotypes predict fatal or nonfatal myocardial infarction: analysis of the scot-heart trial. *Cardiovasc. Imaging* **18**, 308–319 (2025).
47. Yang, A. *et al.* Qwen3 technical report. *arXiv preprint arXiv:2505.09388* (2025).
48. Isensee, F., Jaeger, P. F., Kohl, S. A., Petersen, J. & Maier-Hein, K. H. nnu-net: a self-configuring method for deep learning-based biomedical image segmentation. *Nat. methods* **18**, 203–211 (2021).
49. Salehi, S. S. M., Erdogmus, D. & Gholipour, A. Tversky loss function for image segmentation using 3d fully convolutional deep networks. In *International workshop on machine learning in medical imaging*, 379–387 (Springer, 2017).
50. Lin, T.-Y., Goyal, P., Girshick, R., He, K. & Dollár, P. Focal loss for dense object detection. In *Proceedings of the IEEE international conference on computer vision*, 2980–2988 (2017).
51. Wasserthal, J. *et al.* Totalsegmentator: robust segmentation of 104 anatomic structures in ct images. *Radiol. Artif. Intell.* **5**, e230024 (2023).